ACTA STEREOL 1998; 17/2: 247-252
ORIGINAL SCIENTIFIC PAPER

3D VORONOI TESSELLATIONS GENERATED BY POISSON AND LATTICE CLUSTER FIELDS

Ivan Saxl, Petr Ponížil *

Mathematical Institute, Acad. Sci. of the Czech Republic, Žitná 25, CS-115 67 Praha 1, Czech Republic
*TU Brno, Faculty of Technology, náměstí TGM 275, CS-762 72 Zlín, Czech Republic

ABSTRACT

Spatial Voronoi tessellations generated by cluster fields of the germ-grain type are examined by means of simulations. The grains are Matérn clusters of globular or spherical type and the germ patterns are either the stationary Poisson point process or the cubic lattice. In particular, the effects of the cluster cardinality and size and of the germ arrangement are described and discussed. Simultaneously, the planar induced tessellations are investigated.

Key Words: cluster fields, lattices of clusters, 3D Voronoi tessellation.

INTRODUCTION

Voronoi tessellations of four different cluster fields are investigated in the present paper. They may be considered as the germ-grain models in which the germ (or *parent*) patterns are either the stationary Poisson point process (P) of intensity λ_p or the cubic point lattice (L) of the same intensity and the germs are Matérn point clusters Z (Poisson distributed number N_Z of points – *daughters* – with the mean N) of either globular (G - a uniform random distribution of daughters within a ball of diameter D) or spherical (S – a uniform random distribution of daughters on a sphere of diameter D) type. Or, equivalently, LG, LS are lattices of random clusters in the terminology introduced by Santaló (1976) and PG, PS are Boolean cluster fields. The intensity of cluster fields is $\lambda = N\lambda_p$, the ball size D is expressed by the dimensionless parameter $c_\bullet = D/\rho_p(\bullet)$, where $\rho_p(\bullet)$ is the mean nearest neighbour distance of the parents ($\rho_p(\bullet) = 0.554\lambda_p^{-1/3}$ and $\lambda_p^{-1/3}$ for P and L fields, respectively). The numerical results relate to the unit ($\lambda = 1$) cluster field intensities. Hence, at a given value of $c_L = c_P$, the cluster size is nearly two times greater in the L fields than in the P fields.

A tessellation is described by the distributions of its cell characteristics. The size dependent characteristics are homogeneous functions of degree $-k/3$ of the intensity $\lambda = 1/\mathbf{E}v$, where $k = 3$ for cell volume v, $k = 2$ for cell surface area s, $k = 1$ for cell

Research supported by the Grant Agency of the Czech Republic (contract No. 201/96/0226 – I.S.) and by the Ministry of Education of the Czech Republic (contract No. 96108 – P.P.).

perimeter p and mean cell breadth w. The shape characteristics (mean dihedral angle Θ, randomly selected dihedral angle θ, number of cell faces n and "isoperimetric" shape factors $g = 6v\sqrt{\pi/s^3}, f = 6v/(\pi w^3)$ are independent of λ. Any 3D tessellation induces in a section plane a 2D tessellation of intensity $\lambda' = 1/\mathbf{E}v' = \lambda \mathbf{E}w$. The mean values of its size characteristics (cell area v', perimeter s') obey the stereological relations $\mathbf{E}v' = \mathbf{E}v/\mathbf{E}w$, $\mathbf{E}s' = 0.25\pi \mathbf{E}s/\mathbf{E}w$ and its shape characteristics are edge number $n' = 2/(1 - \mathbf{E}\Theta'/\pi)$, random edge angle θ' and shape factor $f' = 4\pi/s'^2$. Only Matérn globular clusters implanted in parent points of Poisson point process with $N = 5$, 20 and $c \approx 1$, 1.5 have been investigated as yet (Lorz & Hahn, 1993; Van de Weygaert, 1994). As the effects of either daughter number N or cluster size c on cell characteristics are not monotone, a systematic research is needed.

PRELIMINARY CONSIDERATIONS

When the cluster size is very small ($D \ll \rho_p$, *e. g.* $c = 0.005$), the resulting tessellation can be considered nearly as a refinement of the tessellation generated by the parents. The main change produced in the boundaries of parent cells are new edges created along their intersection with the symmetry planes of closely spaced pairs of daughters; the corresponding dihedral angle is close to the value of π and its frequent occurrence gives rise to a pronounced secondary mode in the p.d.f. of the random dihedral angles θ, θ' (Saxl & Ponížil, 1998a, b) – *cf.* Fig. 3b. If clusters are of the S–type, the interior of the parent cells is sliced into pyramid-like daughter cells; nearly each of them has a base formed by a part of the parent cell boundary and, consequently, nearly each daughter has a neighbour belonging to another cluster. Hence the term "*outer*" cells C^O. Clearly $\mathbf{E}v^O = \mathbf{E}v = 1$.

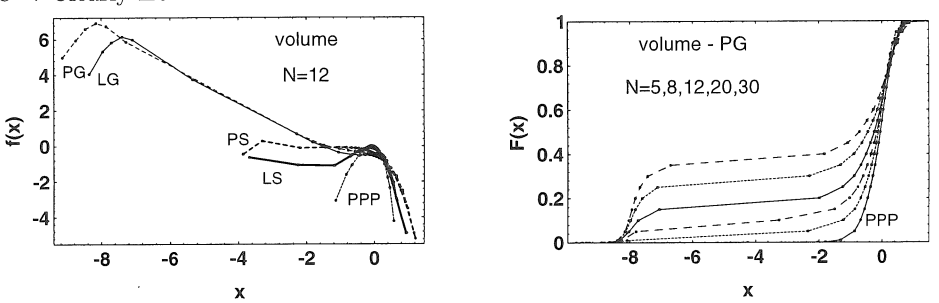

a) b)

Fig. 1 The p.d.f's (a) and distribution functions (b) of the cell volumes v at $c = 0.005$. The ordinate of the plateau estimates the fraction of inner cells α_N.

For clusters of the G–type, the situation is similar only if the cardinality N_Z of the cluster Z is small. However, it may happen starting with $N_Z = 5$ that all neighbours of a point are the points of the same cluster – *sisters* . The cell C^I generated by such a daughter lies completely in the interior of the parent cell and will be called the "*inner*" cell. It was already shown (Saxl & Ponížil, 1998a) that the proportion α_N of inner cells increases with growing N (at $N = 30$ is $p \approx 0.4$ – *cf* Fig. 1b), hence the mean number N^O of outer cells in a cluster is $(1 - \alpha_N)N$ and clearly also $N^I = \alpha_N N$. It can be assumed that the volume of the embedding ball is more or less uniformly distributed between the cells of all daughters: $\mathbf{E}v^I \approx \pi D^3/(6N)$. Then $\mathbf{E}v^I(P) = 0.0283\ c_P^3, \mathbf{E}v^I(L) = 0.166\ c_P^3$ (in the units of $1/\lambda$; note the independence of N!). In

particular, $\mathbf{E}v^I(P) = 3.5 \times 10^{-9}$ and $\mathbf{E}v^I(L) = 2.1 \times 10^{-8}$ for $c_\bullet = 0.005$ examined in what follows (*cf.* Fig. 1a). The mean volume of outer cells must simultaneously increase as their number is $(1-\alpha_N)N$ only, hence $\mathbf{E}v_N^O \approx 1/(1-\alpha_N)$ if the total volume of inner cells is neglected in comparison with the total volume of outer cells. Because of the great difference in size of the outer and inner cells, the moments of the size characteristics are determined mainly by the properties of the former ones. Let $\mu'_j(q_N)$ be the $j-$th general moment of a size property q, which is a homogeneous function of degree $-k/3$ of λ; the index N denotes that the value corresponds to the unit tessellation with $\lambda = N\lambda_p = 1$. Neglecting the contribution of inner cells, $\mu'_j(q_N)^G \approx (1-\alpha_N)\mu'(q_N)^O$. Setting for $\mu'_j(q_N)^O$ the value of $\mu'_j(q_{(1-\alpha_N)N})^S$ estimated from the corresponding S-type tessellation (properly renormalized) we obtain

$$\mu'_j(q_N)^G \approx (1-\alpha_N)^{(1-jk/3)}\mu'_j(q_{(1-\alpha_N)N})^S. \tag{1}$$

In particular,

$$\mathbf{E}s_N^G \approx (1-\alpha_N)^{1/3}\mathbf{E}s_{(1-\alpha_N)N}^S, \tag{2}$$

$$\operatorname{var} v_N^G \approx \frac{1}{1-\alpha_N}(\operatorname{var} v_{(1-\alpha_N)N}^S + 1) - 1. \tag{3}$$

All the above equations apply to L as well as to G cluster fields. Eq. (2) with the exponent 2/3 holds for the size characteristics p_N^G, w_N^G. It can be expected that the repeated similar slicing of parent cells generated by S-clusters will not change the properties of daughter cells considerably. Hence the effect of growing N is mainly due to the power of $(1-\alpha_N)$ and Eqn's (2), (3) explain the differences between tessellations generated by clusters of different type, namely the continual decrease (after an initial maximum) of mean values and a pronounced increase of variances of the cell size characteristics in fields generated by G-clusters.

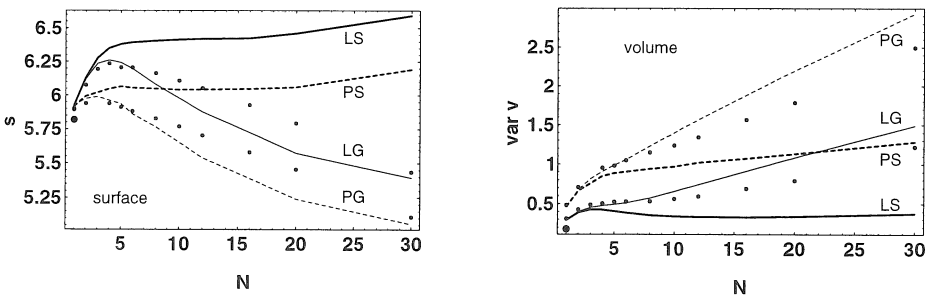

Fig. 2 The mean cell surface s (a) and the variance of the cell volume v(b). The behaviour of the mean width w and of the perimeter p is very similar. The large dot at $N = 1$ denotes the PVT value, small dots show the estimates of PG and LG curves using Eqn's (2), (3).

Let N and the type of cluster be fixed and the different germ arrangement is considered. All parent cells are equal in L-tessellations and the distributions of cell characteristics reflect various possibilities of dividing a slightly corrugated unit cube into cube-filling cells. As q is the homogeneous function of degree $-k/3$ of $\lambda_p = 1/v_p$, the general moment $\mu'^L_j(q(v_p))$ of such a tessellation of a parent cell of volume v_p is

$$\mu'^L_j(q_N(v)) = v_p^{jk/3}\mu'^L_j(q_N(1)). \tag{4}$$

Neglecting the difference in shape between the cubic and Poisson-Voronoi tessellations (PVT), it could be proposed that the division of Poisson-Voronoi cells is quite similar. Then integrating Eq. (4) with respect to cell volume distribution in unit PVT (generalized γ−distribution with $q = 6.289$, $r = 0.889$ and b such that $\mathbf{E}v = 1$)

$$\mu'^{P}_{j}(q_N(v)) \approx \mu'_{jk/3}(v)^{PVT} \times \mu'^{L}_{j}(q_N(1)), \tag{5}$$

where $\mu'_{jk/3}(v)^{PVT}$ is the $jk/3$−th general moment of volume in the unit Poisson-Voronoi tessellation ($\mu'_i(v)^{PVT} = 0.98, 0.98, 1.179$ for $i = 1/3, 2/3, 2$, respectively). The main shortage of this hypothesis is that the generator of the parent cell lies in the cell centre only in lattice tessellations. Consequently, the diversity of daughter cell properties is much greater in tessellations with randomly distributed parents.
An interesting behaviour of the shape characteristics can also be envisaged. For example, the number of faces of inner cells must increase from the value of 4 (tetrahedra) to the value appropriate for PPP (15.53) as the region of inner cells with increasing N approaches a piece of PPP. Consequently, a minimum of $\mathbf{E}n$ at sufficiently high N cannot be excluded even when $\mathbf{E}n$ passes through a maximum at $N \approx 15$ also in tessellations generated by spherical clusters. A more detailed description of the shape characteristics is in Saxl & Ponížil (1998a, b).

RESULTS

The incremental method with the nearest neighbour algorithm (Okabe *et al.*, 1992) was used to construct the Voronoi tessellation associated with point fields of examined types. The tessellations generated by spherical fields would not be normal as the daughter cells have a common vertex in the center of the embedding ball. In order to avoid this, all daughters were given small i.i.d. random shifts ξ; their distribution was 3-variate centred normal with the variance $\sigma^2 I, \sigma = 0.0002\rho_p$, hence 25times smaller than the smallest value of c used. This value ensured reasonable stability of the construction.

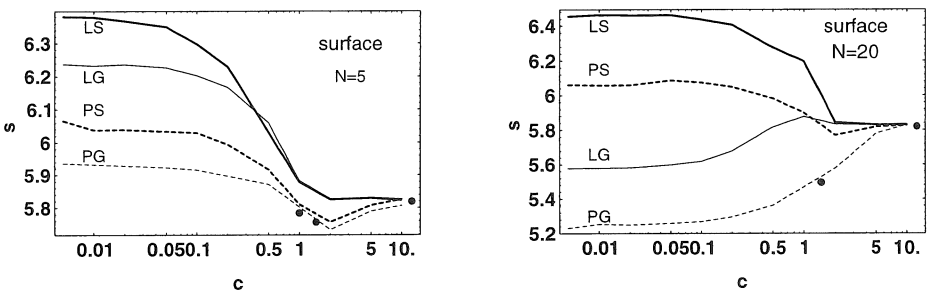

Fig. 3 Mean cell surface s at various cluster sizes for $N = 5$, 20. The dot at $c \approx 13$ denotes the PVT value, the other dots are the results obtained by Lorz & Hahn (1993).

The number of generating points was selected in such a way that after the careful elimination of edge effects about 10^3 cells remained for the analysis. The procedure was then 10^3 times repeated. Consequently, approximately 10^6 polyhedral cells were simulated and examined for any choice of the cluster type (G or S), of the parent pattern type (P,L) and of the parameters $1 \leq N \leq 30$, $0.005 \leq c \leq 10$. Each sample

of size 10^3 was also intersected by several random planes in order to make possible the examination of the induced 2D tessellation, which is not of the Voronoi type. The number of intersecting planes was such that the number of profiles per sample was about 2.10^3, which resulted in the total number of examined profiles about 2.10^6 in each considered case.

a. Effect of the number of daughters. The presence and size of inner cells are demonstrated in Fig. 1a, their fraction α_N can be deduced from Fig. 1b ($\alpha_N \approx 0.0133N$). The inequalities $\mathbf{E} \bullet (LS) \geq \mathbf{E} \bullet (PS)$, $\mathbf{E} \bullet (LG) \geq \mathbf{E} \bullet (PG)$ are obeyed by all size characteristics in agreement with Eq. (5) - however crude are the assumptions used to deduce it, the observed ratio $s_N^L/s_N^P \approx 0.93$ is of the same order and sense as the prediction (0.98). The inequalities $\mathbf{E} \bullet (LS) \geq \mathbf{E} \bullet (LG)$, $\mathbf{E} \bullet (PS) \geq \mathbf{E} \bullet (PG)$ as well as the occurrence of maxima on LG and PG curves are in agreement (even numerically – *cf.* Fig. 2a)) with the prediction of Eq. (2). The maxima are shifted to lower values of N as clusters with $N_Z \geq 5$ are present in sufficient quantity already at $N = 3$ (10%) and 4 (15%).

Reverted inequalities var $\bullet (LS) \leq$ var $\bullet (LG)$, var $\bullet (PS) \leq$ var $\bullet (PG)$ (*cf.* Fig.2b and similarly for var p, var w) are the consequences of Eq'ns (3),(1). The values of variances are slightly underestimated by Eq. (3) – *cf.* Fig. 2b. Eq. (5) correctly predicts higher values of variances in P–tessellations than in L–tessellations, but the estimates are only about 50% of the true values.

b. Effect of cluster size. Three characteristic sizes of clusters can be defined. Let $\lambda_{cl} = N/(\kappa R^d)$ be the local intensity of daughters in the cluster. A cluster is said to be *dissolved* if $\lambda_{cl} \approx \lambda$; the corresponding cluster sizes are $c_{dis}^P \approx 2.3, c_{dis}^L \approx 1.2$. Other two measures of cluster size are based on the concept of cluster interaction. Using the formula for the void probability (Stoyan et al., 1995), the probabilities p_1 of the intersection of two cluster embedding balls and p_2 of their mutually including their centres can be found (Saxl & Kohútek, 1997). Then at $c \leq c_0^P = 0.5$ the inequalities $p_1 \leq 0.1, p_2 \leq 0.01$ hold whereas $c \geq c_\infty^P = 4$ implies $p_1, p_2 \approx 1$. Similarly, at $c < c_0^L = 1$ are $p_1 = p_2 = 0$ and at $c \geq c_\infty^L = 2$ are $p_1 = p_2 = 1$.

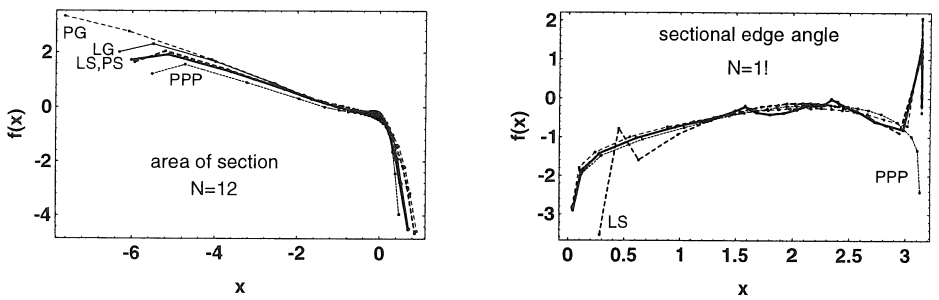

a) b)

Fig. 4 The p.d.f's of sectional characteristics v' (a) and θ' (b). Note a pronounced mode near $x = \pi$ present already at $N = 1$ and further modes in sections of L-tessellations (thick line – LG).

The effect of cluster size differs in four considered cases – Fig. 3. The values of the size parameters fullfil the inequalities $\mathbf{E} \bullet (LS) \geq \mathbf{E} \bullet (LG)$, $\mathbf{E} \bullet (PS) \geq \mathbf{E} \bullet (PG)$ at small values of N (*cf.* Fig. 2a) and they all decrease to the limit value of $\mathbf{E} \bullet (PVT)$ with growing c. The changes proceed first (below c_0) within the parent cells (the

inner cells grow and the outer ones diminish), then the interaction of clusters prevails. The passage to PVT is not monotone only in the vicinity of c_{dis} and c_{∞} (*cf.* Fig. 3). At higher values of N, the size characteristics either decrease (L-fields) or increase (G-fields). Note that Lorz & Hahn (1993) could not observe different behaviour at $N = 5$ and $N = 20$ because of too great size of their clusters. More detailed results can be obtained by analysing p.d.f's and will be published elsewhere.

c. Planar sections. Many above discussed features are lost or hardly distinguishable in the planar sections of 3D tessellations. As $\mathbf{E}v' = 1/\mathbf{E}w$ and there is no substantial difference in the plots $\mathbf{E}s$ *vs* N and $\mathbf{E}w$ *vs* N, the order of curves in $\mathbf{E}v'$ *vs* N is reversed and minima are observed instead of maxima. From similar reasons, lattice and Poisson fields cannot be distinguished in the plots $\mathbf{E}s'$ *vs* N. Also the p.d.f's of cell characteristics are rather similar (*cf.* Fig. 4a) and different fields can be hardly distinguished in practice when the resolution power and the accuracy of measurements are much lower then in computer simulations. Variances of cell areas are perhaps the most sensitive quantities (Lorz, 1990; Hahn & Lorz, 1994), unfortunately crossing of curves occurring in Fig. 2b is repeated also in the corresponding sectional plot var v' *vs* N.

A strong qualitative proof of clustering is the secondary mode of the edge angle θ' (*cf.* Fig. 4b) prominent even at $N = 1$; however, it cannot be used to differentiate between the considered cluster fields as it is incited by outer cells. In L-tessellations, also other modes typical for sections of cubic tessellations are visible at low values of N – Fig. 4b.

REFERENCES

Hahn U, Lorz U: Stereological analysis of the spatial Poisson-Voronoi tessellation. J Microsc 1994; 175: 176-185.

Lorz U: Cell-area distributions of planar sections of spatial Voronoi mosaics. Materials Characterization 1990; 25: 297-311.

Lorz U, Hahn U: Geometric characteristics of random spatial Voronoi tessellations and planar sections. Preprint 93-05. Freiberg: Bergakademie Freiberg, 1993.

Okabe A, Boots B, Sugihara K: Spatial tessellations. Chichester: J Wiley & Sons, 1992.

Santaló, LA: Integral Geometry and Geometric Probability. Addison-Wesley Publ Comp, Reading (Mass.), 1976.

Saxl I, Kohútek I: Voronoi tessellations generated by Boolean cluster fields. In: Wojnar L, Rożniatowski K, Kurzydłowski K(eds.): Proc Int Conf on The Quantitative Description of Materials Microstructure. Warsaw, April 1997, 481-488.

Saxl I, Ponížil, P: Estimation of properties of polycrystalline grain structure. In: L Parilák: Fractography 97. Proc Int Conf, Vysoké Tatry, ÚMV SAV Košice 1997, 132-144.

Saxl I, Ponížil P (a): 3D Voronoi tessellations of cluster fields. Acta Stereol 1998 (in press).

Saxl I, Ponížil P (b): Shapes of Voronoi polytops. In: M Hušková, P Lachout, JÁ Víšek (eds): Proc Int Conf "Prague Stochastics '98", JČMF, Praha 1998, 505-10.

Stoyan D, Kendall WS, Mecke J: Stochastic Geometry and its Applications. New York: J Wiley & Sons, 1995.

Van de Weygaert R: Fragmenting the universe III. Astron Astrophys 1994; 283: 361-406.

Presented at the 7th European Congress for Stereology, Amsterdam, April 20th to 23rd, 1998.